Identifying the active flow regions that drive linear and nonlinear instabilities

Olivier Marquet[1] **& Lutz Lesshafft**[2]

[1]ONERA/DAFE, 8 rue des Vertugadins, 92190 Meudon, France
[2]Laboratoire d'Hydrodynamique, CNRS/École polytechnique, 91128 Palaiseau, France

A new framework for the analysis of unstable oscillator flows is explored. In linear settings, temporally growing perturbations in a non-parallel flow represent unstable eigenmodes of the linear flow operator. In nonlinear settings, self-sustained periodic oscillations of finite amplitude are commonly described as nonlinear global modes. In both cases the flow dynamics may be qualified as being *endogenous*, as opposed to the exogenous behaviour of amplifier flows driven by external forcing. This paper introduces the *endogeneity* concept, a specific definition of the sensitivity of the global frequency and growth rate with respect to variations of the flow operator. The endogeneity, defined both in linear and nonlinear settings, characterizes the contribution of localized flow regions to the global eigendynamics. It is calculated in a simple manner as the local point-wise inner product between the time derivative of the direct flow state and an adjoint mode. This study demonstrates for two canonical examples, the Ginzburg–Landau equation and the wake of a circular cylinder, how an analysis based on the endogeneity may be used for a physical discussion of the mechanisms that drive a global instability. The results are shown to be consistent with earlier 'wavemaker' definitions found in the literature, but the present formalism enables a more detailed discussion: a clear distinction is made between oscillation frequency and growth rate, and individual contributions from the various terms of the flow operator can be isolated and separately discussed. In particular, in the context of nonlinear saturated oscillations in the cylinder wake, such an analysis allows to discriminate between the quasi-linear dynamics of fluctuations around a time-averaged mean flow on one hand and the effect of harmonic interactions on the other hand; the results elucidate why a linear analysis of the mean flow in this particular case provides accurate predictions of the nonlinear dynamics.

1. Introduction

Global instability in flows denotes the possibility of a spontaneous bifurcation from a steady flow state to a time-periodic state of synchronised oscillations in the entire flow field. A commonly observed scenario is that of a supercritical Hopf bifurcation, where linearly unstable perturbations of small amplitude first experience exponential growth, until nonlinear effects lead to amplitude saturation. The final time-periodic flow state is named a nonlinear global mode (Huerre & Monkewitz 1990); the exponentially growing small-amplitude perturbations in the early stage of the bifurcation correspond to eigenmodes of the linearized flow operator, traditionally called linear global modes. The attribute *global* is used here to designate an analysis that resolves all non-homogeneous flow directions, as opposed to a *local* Ansatz, which implies the approximation of locally parallel flow.

Nonlinear global modes are usually obtained as asymptotic oscillatory states from time-resolved numerical simulations, whereas linear global mode analysis requires the solution

of linear eigenvalue problems. Complex eigenvalues represent the temporal growth rate and the oscillation frequency; the associated eigenfunctions characterize the spatial distribution of fluctuation amplitude and phase. Linear global mode analysis is now routinely applied to two- and three-dimensional flow configurations. Beyond the primary question whether or not perturbations at small amplitude are unstable, a physical discussion of linear global modes is usually centered around two questions: (i) what are the physical mechanisms that give rise to unstable growth, and (ii) by what means can instability be reduced or enhanced? The first of these questions addresses the endogenous (or intrinsic) flow behaviour, the second question concerns the control of those dynamics through exogenous (or extrinsic) manipulation.

Huerre & Monkewitz (1990) describe the conceptual notion of a 'wavemaker' (a word first used by Monkewitz 1990) as the region where instability waves are intrinsically generated in globally unstable flows. The interpretation by Koch (1985) of global instability in a wake already uses the same principal idea. Chomaz *et al.* (1991) derive a formal criterion for the global frequency selection in the context of the linear Ginzburg–Landau equation, based on the local absolute instability properties. Their formalism is rooted in a WKBJ approximation of instability wavepackets developing in a weakly non-parallel open flow. Within this approximation, local instability waves with upstream- and downstream-oriented group velocity emanate from a streamwise station, the 'wavemaker' location, where the two mode branches can be matched by means of a non-physical analytic continuation of the dispersion relation, defined as a function of a complex spatial x-coordinate. Such intrinsically generated waves grow and decay as they propagate. While the localized 'wavemaker' selects the frequency and drives the global instability mode, it is in general not characterized by large oscillation amplitudes. The spatial separation of the region where waves are generated and the region where they reach their maximal amplitude is caused by convective instability mechanisms in a local sense, or by the non-normality of the linear Navier–Stokes operator in a global sense (Cossu & Chomaz 1997).

A quantitative theory of frequency selection in *nonlinear* systems, still based on the assumption of slow streamwise flow development and for the Ginzburg–Landau model equation, has been proposed by Couairon & Chomaz (1997) and by Pier *et al.* (1998). These studies draw on the theory of front dynamics (van Saarlos 1988, 1989), leading to the simple criterion that the nonlinear global mode frequency is given to first order by the absolute frequency at the upstream boundary of a (locally) absolutely unstable flow region of finite extent. Subsequent applications to wake flows (Pier & Huerre 2001; Pier 2002; Chomaz 2003) suggest that the accuracy of this criterion is only limited by the non-parallelism of the base flow over the distance of amplitude saturation. The transition from (upstream) convective to (downstream) absolute instability marks the 'wavemaker' location within the framework of this nonlinear model.

Linear global modes in non-parallel flows may now be computed directly, without the need for the hypothesis of slow streamwise development. However, the notion of a cause-and-effect relation between different streamwise regions is lost along with this approximation, and the localisation of a 'wavemaker' region within a global structure must be accomplished through new criteria. The *sensitivity* of the linear eigenvalue (frequency and growth rate) with respect to localized changes of the flow operator provides the appropriate concepts for a formal definition of a global 'wavemaker'. Yet the sensitivity problem may be posed in several ways, depending on the physical premise of what 'drives' an instability.

Giannetti & Luchini (2007) provide a discussion of the cylinder wake instability based on the structural sensitivity of the unstable linear eigenmode. The structural sensitivity,

in their definition, quantifies how an eigenvalue is affected by the introduction of localized forcing of a given perturbation quantity, proportional in strength to the same or another perturbation quantity. It thereby provides a measure in every point in space for the effect of internal feedback between perturbations. Giannetti & Luchini (2007) conjecture that those regions where an altered coupling induces the strongest change of the eigenvalue must also be the most significant regions for the action of internal feedback mechanisms that underpin the genuine eigenmode dynamics. At present, this formalism is arguably the most commonly accepted definition of the 'wavemaker' in a global analysis framework. The concept is quite naturally extended to nonlinear global modes by way of Floquet theory (Luchini *et al.* 2008). However, one inconvenience of this approach is that it does not distinguish between frequency and growth rate, as the Cauchy–Schwarz theorem is invoked in order to define an upper bound for the drift of the *modulus* of the eigenvalue. Another stems from the large number of feedback relations between the various flow quantities that may prove to be significant. The formalism does not allow to single out the influence of specific terms in the flow equations.

Marquet *et al.* (2008) investigate the sensitivity of the linear cylinder wake instability with respect to localized modifications of the base flow. As far as linear instability is linked to the interaction between perturbations and the base flow, it may be argued that such an analysis is well suited to identify the principal flow regions where instability originates. The formalism distinguishes between frequency and growth rate, yet it is clearly cast in the form of a *control* problem. The question how an instability mode is affected by *exogenous* alterations, be it alterations of the internal feedback (Giannetti & Luchini 2007) or of the base flow (Marquet *et al.* 2008), is conceptually different from the question how its *endogenous* dynamics come into being.

The objective of the present paper is to propose a variant of the sensitivity problem for linear as well as nonlinear global modes that identifies more directly those endogenous eigendynamics. For the sake of comparison and validation, these concepts are demonstrated for the two traditional test settings used in the literature on wavemakers: the one-dimensional Ginzburg–Landau equation and the two-dimensional cylinder wake. It is hoped that the formalism will be useful for the analysis of physical instability phenomena in a wide range of applications.

The paper is organised as follows. Section 2 documents linear and nonlinear global mode results for the Ginzburg–Landau equation and for the cylinder wake. This section does not contain genuinely new results, but rather serves as a repertory and review. The configurations discussed here are used in the following as examples in order to demonstrate the proposed formalism. The endogeneity concept is introduced for linear settings in §3, and its application for the analysis of linear global modes is demonstrated for the two example configurations. The extension of the formalism to fully nonlinear situations is laid out in §4. Conclusions are given in §5. An appendix addresses the implications of general inner products for the analysis.

2. Linear, nonlinear, direct and adjoint global modes

The evolution equation of a flow variable $\mathbf{q}(\mathbf{x}, t)$ is considered in the general form

$$\mathcal{B}\, \partial_t \mathbf{q} = \mathcal{N}(\mathbf{q}) \,, \tag{2.1}$$

where $\mathcal{N}$ is a nonlinear operator, and $\mathcal{B}$ is an operator of very simple structure that indicates on which component of $\mathbf{q}$ the time derivative applies. In what follows, it will always be assumed that $\mathcal{B}$ is self-adjoint.

A base flow $\mathbf{q}_b$ is a steady solution of the nonlinear equation, $\mathcal{N}(\mathbf{q}_b) = 0$. The linear stability of such a steady base flow is investigated by superposing small-amplitude time-dependent perturbations $\mathbf{q}'$. The dynamics of these perturbations is governed by the linear equation

$$\mathcal{B}\,\partial_t \mathbf{q}' = \mathcal{L}_{\mathbf{q}_b}\mathbf{q}'\,, \qquad (2.2)$$

where the linear operator $\mathcal{L}_{\mathbf{q}_b}$ is obtained as the linearisation of $\mathcal{N}$ around the base flow: $\mathcal{N}(\mathbf{q}_b + \epsilon\mathbf{q}') = \mathcal{N}(\mathbf{q}_b) + \epsilon\mathcal{L}_{\mathbf{q}_b}\mathbf{q}'$. Eigenvalues λ_j and associated eigenfunctions $\boldsymbol{\phi}_j(\mathbf{x})$ of $\mathcal{L}_{\mathbf{q}_b}$ are obtained as solutions of the eigenvalue problem

$$\lambda_j\,\mathcal{B}\,\boldsymbol{\phi}_j = \mathcal{L}_{\mathbf{q}_b}\boldsymbol{\phi}_j\,. \qquad (2.3)$$

The eigenmodes $\mathbf{q}'_j(\mathbf{x}, t) = \boldsymbol{\phi}_j(\mathbf{x})\exp(\lambda_j t)$ form a complete basis for the range of $\mathcal{L}_{\mathbf{q}_b}$. In physical terms, the real and imaginary parts of a complex eigenvalue represent temporal growth rate σ and frequency ω of a linear eigenmode. The convention $\lambda = \sigma - \imath\omega$ is adopted here, i.e. the frequency is given by the negative imaginary part of λ.

For the purpose of deriving an adjoint equation associated with the direct equation (2.2), the following inner product of vector-valued functions is introduced:

$$\{\boldsymbol{f}(\mathbf{x}, t), \boldsymbol{g}(\mathbf{x}, t)\} = \int_0^T \int_\Omega \boldsymbol{f}^*(\mathbf{x}, t) \cdot \boldsymbol{g}(\mathbf{x}, t)\,\mathrm{d}\mathbf{x}\,\mathrm{d}t\,, \qquad (2.4)$$

where the star denotes the complex conjugate. The adjoint linear operator $\mathcal{L}_{\mathbf{q}_b}^\dagger$ is then derived by requiring

$$\left\{\mathbf{q}^\dagger, \mathcal{B}\,\partial_t \mathbf{q}' - \mathcal{L}_{\mathbf{q}_b}\mathbf{q}'\right\} = \left\{-\mathcal{B}\,\partial_t \mathbf{q}^\dagger - \mathcal{L}_{\mathbf{q}_b}^\dagger\mathbf{q}^\dagger, \mathbf{q}'\right\}\,. \qquad (2.5)$$

The adjoint equation associated with (2.2) is thus found as

$$-\mathcal{B}\,\partial_t \mathbf{q}^\dagger = \mathcal{L}_{\mathbf{q}_b}^\dagger\mathbf{q}^\dagger\,. \qquad (2.6)$$

The linear adjoint operator has eigenmodes $\mathbf{q}_j^\dagger(\mathbf{x}, t) = \boldsymbol{\phi}_j^\dagger(\mathbf{x})\exp(\lambda_j^* t)$. Adjoint eigenvalues λ_j^* are the complex conjugate values of the corresponding direct eigenvalues λ_j. Adjoint eigenfunctions $\boldsymbol{\phi}_j^\dagger(\mathbf{x})$ satisfy

$$\lambda_j^*\,\mathcal{B}\,\boldsymbol{\phi}_j^\dagger = \mathcal{L}_{\mathbf{q}_b}^\dagger\boldsymbol{\phi}_j^\dagger\,. \qquad (2.7)$$

The direct and adjoint eigenfunctions form biorthogonal sets,

$$\langle\boldsymbol{\phi}_j^\dagger, \mathcal{B}\boldsymbol{\phi}_k\rangle = \delta_{jk}\,, \qquad (2.8)$$

with respect to the purely spatial inner product

$$\langle\boldsymbol{f}(\mathbf{x}), \boldsymbol{g}(\mathbf{x})\rangle = \int_\Omega \boldsymbol{f}^*(\mathbf{x}) \cdot \boldsymbol{g}(\mathbf{x})\,\mathrm{d}\mathbf{x}\,. \qquad (2.9)$$

In the definition of Huerre & Monkewitz (1990), a *nonlinear* global mode is a time-periodic solution of the nonlinear evolution equation (2.1), denoted here by $\mathbf{q}_0(\boldsymbol{x}, t)$. In the examples considered in the present investigation, such a nonlinear global mode is the limit-cycle solution that is reached as the result of amplitude saturation of an initially growing linear eigenmode. The nonlinear global mode has a real-valued global frequency $\omega_g = 2\pi/T$, with T being the cycle period.

The linear stability of this time-periodic solution is investigated by considering the temporal evolution of small perturbations $\mathbf{q}'(\mathbf{x}, t)$, governed by the linear equation

$$\mathcal{B}\,\partial_t \mathbf{q}'(\boldsymbol{x}, t) = \mathcal{L}_{\mathbf{q}_0(t)}\,\mathbf{q}'(\boldsymbol{x}, t)\,. \qquad (2.10)$$

The tangential linear operator $\mathcal{L}_{\mathbf{q}_0(t)}$ is obtained by linearizing the nonlinear operator $\mathcal{N}$ around the time-periodic solution $\mathbf{q}_0(t)$. As $\mathcal{L}_{\mathbf{q}_0(t)}$ is also time-periodic, a fundamental set of solutions to (2.10) is given by $\boldsymbol{\psi}_j(\mathbf{x}, t) \exp(\zeta_j t)$ (see Iooss & Joseph 1997). The Floquet modes $\boldsymbol{\psi}_j(\mathbf{x}, t)$ are T-periodic in time, and the associated Floquet multipliers $\exp(\zeta_j T)$ characterize the temporal growth or decay of a mode over one cycle period. The real part of ζ_j is in fact the Lyapunov exponent, the imaginary part of ζ_j corresponds to a variation of the fundamental frequency.

An interesting property is that the time derivative of the time-periodic solution, $\partial_t \mathbf{q}_0$, is a neutral Floquet mode of the autonomous periodic operator $\mathcal{L}_{\mathbf{q}_0(t)}$. This property results from the phase invariance of the time-periodic solution. Both $\mathbf{q}_0(\mathbf{x}, t)$ and $\mathbf{q}_0(\mathbf{x}, t + \delta t)$ represent T-periodic solutions of the nonlinear equation (2.1), therefore their difference $\delta \mathbf{q} = \mathbf{q}_0(\mathbf{x}, t + \delta t) - \mathbf{q}_0(\mathbf{x}, t)$ is T-periodic as well. A Taylor expansion for small δt gives $\delta \mathbf{q} = \partial_t \mathbf{q}_0(\mathbf{x}, t) \delta t$. It follows that $\partial_t \mathbf{q}_0(\mathbf{x}, t)$ is a T-periodic solution of (2.10), and is therefore a *neutral* Floquet mode:

$$\boldsymbol{\psi}_1(\mathbf{x}, t) = \partial_t \mathbf{q}_0(\mathbf{x}, t), \quad \zeta_1 = 0. \tag{2.11}$$

An adjoint tangential operator $\mathcal{L}^{\dagger}_{\mathbf{q}_0(t)}$ can also be defined by requiring

$$\left\{ -\mathcal{B} \partial_t \mathbf{q}^{\dagger} - \mathcal{L}^{\dagger}_{\mathbf{q}_0(t)} \mathbf{q}^{\dagger}, \mathbf{q}' \right\} = \left\{ \mathbf{q}^{\dagger}, \mathcal{B} \partial_t \mathbf{q}' - \mathcal{L}_{\mathbf{q}_0(t)} \mathbf{q}' \right\}, \tag{2.12}$$

from where follows the adjoint equation associated with (2.10),

$$-\mathcal{B} \partial_t \mathbf{q}^{\dagger}(\mathbf{x}, t) = \mathcal{L}^{\dagger}_{\mathbf{q}_0(t)} \mathbf{q}^{\dagger}(\mathbf{x}, t). \tag{2.13}$$

The linear operator $\mathcal{L}^{\dagger}_{\mathbf{q}_0(t)}$ is also T-periodic. Equation (2.13) has fundamental solutions in the form of adjoint Floquet modes $\boldsymbol{\psi}^{\dagger}_j(\mathbf{x}, t) \exp(\zeta_j^* t)$. The sets $\boldsymbol{\psi}^{\dagger}_j$ and $\boldsymbol{\psi}_k$ are again biorthogonal, with respect to the spatio-temporal inner product (2.4), such that with a suitable normalisation they fulfill

$$\{\boldsymbol{\psi}^{\dagger}_j, \mathcal{B} \boldsymbol{\psi}_k\} = \delta_{jk}. \tag{2.14}$$

Only the adjoint Floquet mode $\boldsymbol{\psi}^{\dagger}_1$ associated with the neutral Floquet mode $\boldsymbol{\psi}_1$ and $\zeta_1 = 0$ will be used in the following analysis.

2.1. *Ginzburg–Landau equation*

The Ginzburg–Landau equation has often served as a simple model for flow instability dynamics (Huerre 2000). Its scalar state variable $q(x, t)$ only depends on one spatial coordinate, yet its dispersion relation permits a double branch point that allows to distinguish between absolutely and convectively unstable situations, analogous to open shear flows. The nonlinear Ginzburg–Landau equation is used here in the form

$$\partial_t q = \mathcal{N}(q) = -U \partial_x q + \mu(x) q + \gamma \partial_{xx} q - \beta |q|^2 q. \tag{2.15}$$

The operator $\mathcal{B}$, in the general notation (2.1), in this case is simply the identity, and the operator $\mathcal{N}$ is given by the right-hand side in (2.15). It is composed of terms representing convection, linear reactive sources, diffusion, and cubic nonlinearity. Following Cossu & Chomaz (1997), constant convection and diffusion parameters are chosen, $U = 6$ and $\gamma = 1 - i$, while a parabolic variation of the reactive parameter is prescribed as

$$\mu(x) = \mu_0 + 0.5 \mu_2 x^2. \tag{2.16}$$

Different values of μ_0 will be used in the following, while $\mu_2 = -0.1$ is maintained throughout. This variation yields a strong local stability of the system far from $x = 0$.

All following calculations are performed on an interval $x \in [-40, 40]$, and in all cases the fluctuation amplitudes are indeed negligibly small at the numerical boundaries. The nonlinearity parameter is chosen as $\beta = 1 - \imath$, except when linear situations $\beta = 0$ are considered.

2.1.1. *Linear Ginzburg–Landau*

Note that the zero state $q \equiv 0$ is a steady solution of the nonlinear Ginzburg–Landau equation (2.15). Linearisation around that state yields the linear Ginzburg–Landau equation

$$\partial_t q = \mathcal{L}q = -U\partial_x q + \mu(x)q + \gamma\partial_{xx}q, \tag{2.17}$$

which is equivalent to (2.15) with $\beta = 0$. A subscript 0 could be attached to $\mathcal{L}$, denoting the zero base state, but this will be omitted in the following. The associated adjoint operator is obtained as

$$\mathcal{L}^\dagger q^\dagger = U\partial_x q^\dagger + \mu(x)q^\dagger + \gamma^*\partial_{xx}q^\dagger. \tag{2.18}$$

As derived by Chomaz *et al.* (1987), the leading eigenmodes of the direct problem $\lambda\phi = \mathcal{L}\phi$ and of the adjoint problem $\lambda^*\phi^\dagger = \mathcal{L}^\dagger\phi^\dagger$ are found as

$$\lambda = \mu_0 - \frac{U^2}{4\gamma} - \sqrt{\frac{-\mu_2\gamma}{2}}, \tag{2.19}$$

$$\phi(x) = \exp\left(\frac{Ux}{2\gamma} - \sqrt{\frac{-\mu_2}{2\gamma}}\frac{x^2}{2}\right), \tag{2.20}$$

$$\phi^\dagger(x) = \exp\left(-\frac{Ux}{2\gamma^*} - \sqrt{\frac{-\mu_2}{2\gamma^*}}\frac{x^2}{2}\right). \tag{2.21}$$

For fixed values of U, γ and μ_2, the real-valued parameter μ_0 completely determines the eigenvalue, but it has no influence on the eigenfunction shape. The direct and adjoint eigenfunctions are shown in figure 1. Their maxima are located at $x = 8.6$ and $x = -8.6$, respectively. According to Cossu & Chomaz (1997), global instability arises when $\mu_0 > \mu_c$, with a critical value

$$\mu_c = \frac{U^2}{4|\gamma|^2} + \left|\sqrt{\frac{-\mu_2\gamma}{2}}\right|\cos\left(\frac{\arg\gamma}{2}\right). \tag{2.22}$$

The local instability properties are given by Chomaz *et al.* (1988). The model is locally stable wherever $\mu(x) < 0$, convectively unstable for $0 < \mu(x) < U^2/4|\gamma|^2$ and absolutely unstable for $\mu(x) > U^2/4|\gamma|^2$. The extent of these regions depends on the value of μ_0.

2.1.2. *Nonlinear Ginzburg–Landau*

Pier *et al.* (1998) report that the Hopf bifurcation in a nonlinear Ginzburg–Landau system is supercritical. Nonlinear global instability therefore follows from linear global instability, $\mu_0 > \mu_c$, and the nonlinear global mode emerges after saturation of the growing linear global mode. A strongly supercritical setting is considered here, with $\mu_0 = 2\mu_c$.

The direct nonlinear global mode is computed by time-stepping (2.15), starting from the linear global mode shape (2.20) as an initial perturbation at low amplitude, until an asymptotic time-periodic state q_0 is reached. The linearisation of Equation (2.15) around the oscillating state q_0 is accomplished as detailed in Hwang (2015). The nonlinear term $\beta|q|^2q$ is properly linearized by augmenting the complex state variable with its complex conjugate, i.e. writing out the nonlinear and linear equations in terms of state vectors $(q, q^*)^T$. In the present study, the direct linear equation is in fact never needed, except
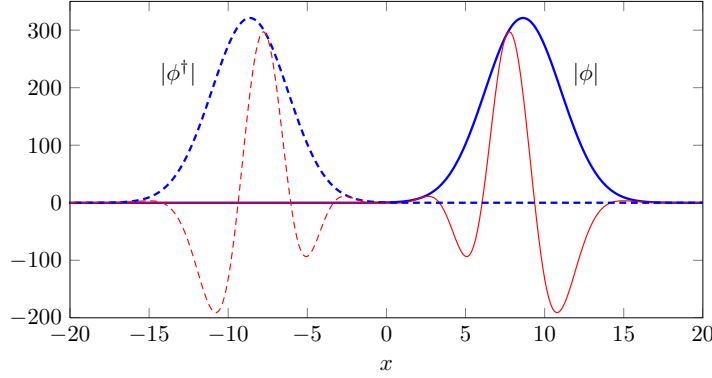
FIGURE 1. Direct and adjoint eigenfunctions (2.20, 2.21) of the linear Ginzburg–Landau equation. Absolute values are shown as thick blue lines, real parts as thin red lines. Solid lines represent the direct mode, dashed lines represent the adjoint mode. The scaling is such that $\langle \phi^\dagger, \phi \rangle = 1$.

for the derivation of the adjoint linear equation,

$$- \partial_t q^\dagger - U \partial_x q^\dagger - \mu q^\dagger - \gamma^* \partial_{xx} q^\dagger - 2\beta^* |q_0(t)|^2 q^\dagger + \beta^* q_0^2(t) q^{\dagger *} = 0 \,. \tag{2.23}$$

With the known time-periodic solution $q_0(t)$, this equation is numerically integrated backward in time, until convergence towards a periodic solution $q_1^\dagger$ is reached. The existence of such an asymptotic solution is guaranteed, because this is the adjoint Floquet mode associated with the neutral direct Floquet mode q_1, defined as the time-derivative of the nonlinear time periodic solution $q_1 = \partial_t q_0$. Details on Floquet theory can be found in Iooss & Joseph (1997).

A Crank–Nicolson scheme is used for the time integration of the nonlinear direct and the associated linear adjoint problem. The use of upwinding finite-difference stencils (seven points) for the spatial discretisation of the direct problem, and downwinding for the adjoint problem, is essential in order to achieve the required numerical accuracy.

Figure 2(a) shows the nonlinear global mode q_0 as it is recovered after transients have disappeared. The amplitude envelope has the emblematic shape of an 'elephant' mode (Pier *et al.* 1998), with a sharp upstream wavefront and a softer downstream decay. According to WKBJ theory, the front should be situated at the upstream boundary of the absolutely unstable region in x. In the present case, absolute instability prevails in the interval $x \in [-10, 10]$, and the foot of the front is indeed placed around $x = -10$. The adjoint Floquet mode, represented in figure 2(b), has significant amplitudes only upstream of the direct wavepacket, with a maximum near $x = -13$.

It is to be noted that the nonlinear global mode of the Ginzburg–Landau equation only contains one single frequency, because the nonlinear term is of such a form that it does not generate harmonics. As a result, the time signal in each point shows pure sinusoidal oscillations with zero mean. This property proves to be very convenient for all further discussion, whereas the harmonics and the non-zero mean oscillations that are characteristic for the nonlinear dynamics of the Navier–Stokes equations add further complexity to the analysis (see §4.4).

2.2. *Two-dimensional cylinder wake*

The wake of a cylinder is the most commonly used example of an oscillator-type shear flow. The critical Reynolds number for onset of self-sustained vortex shedding, $Re_c = 47$ according to the experiments by Provansal *et al.* (1987), has been repeatedly recovered
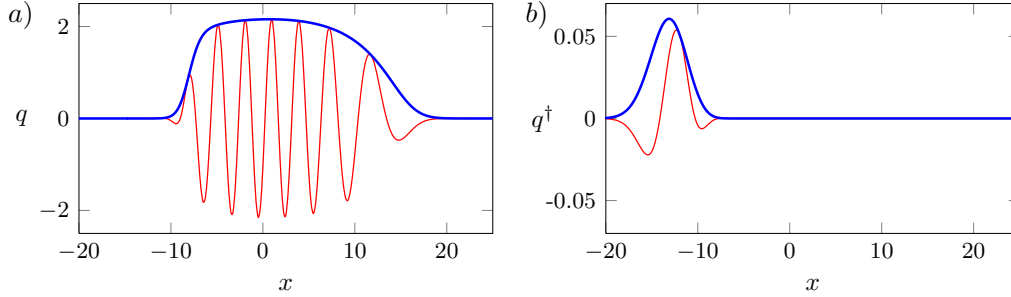
FIGURE 2. *a*) Direct nonlinear global mode of the Ginzburg–Landau equation, with parameters as given in the text. Thick blue line: amplitude envelope; thin red line: snapshot of the real part of q. *b*) Associated neutral adjoint Floquet mode. Same line styles as in *a*.

with high precision as the critical value for the onset of linear global instability (see for instance Barkley 2006; Sipp & Lebedev 2007). Furthermore, the nonlinear global instability of wakes is rather accurately predicted by local theory (Pier 2002; Chomaz 2003). The cylinder wake has been chosen to illustrate the sensitivity studies by Giannetti & Luchini (2007), by Marquet *et al.* (2008), by Luchini *et al.* (2008) and by Luchini & Bottaro (2014). The case at $Re = 80$, well above the instability threshold, is considered in the present study.

In the general notation (2.1), the state vector $\mathbf{q} = (\boldsymbol{u}, p)$ now gathers the velocity vector and the pressure field, which together satisfy the incompressible Navier-Stokes equations, and the operators $\mathcal{B}$ and $\mathcal{N}$ are defined by

$$\mathcal{B} = \begin{pmatrix} \mathcal{I} & 0 \\ 0 & 0 \end{pmatrix} , \quad \mathcal{N}(\mathbf{q}) = \begin{pmatrix} -(\mathbf{u} \cdot \boldsymbol{\nabla})\mathbf{u} - \boldsymbol{\nabla}p + Re^{-1}\boldsymbol{\Delta}\mathbf{u} \\ \boldsymbol{\nabla} \cdot \mathbf{u} \end{pmatrix} . \tag{2.24}$$

2.2.1. *Linear instability of the cylinder wake*

The cylinder wake problem permits a non-trivial steady solution $\mathbf{q}_b = (\mathbf{u}_b, p_b)$, satisfying $\mathcal{N}(\mathbf{q}_b) = \mathbf{0}$, which will serve as a base flow. Linear perturbations $\mathbf{q}' = (\mathbf{u}', p')$ developing on this base flow are governed by the linear equations (2.2) with

$$\mathcal{L}_{\mathbf{q}_b}\mathbf{q}' = \begin{pmatrix} -(\mathbf{u}_b \cdot \boldsymbol{\nabla})\mathbf{u}' - (\mathbf{u}' \cdot \boldsymbol{\nabla})\mathbf{u}_b + Re^{-1}\boldsymbol{\Delta}\mathbf{u}' - \boldsymbol{\nabla}p' \\ \boldsymbol{\nabla} \cdot \mathbf{u}' \end{pmatrix} . \tag{2.25}$$

Eigenmodes of this linear operator are obtained numerically as described in Sipp & Lebedev (2007). Only one unstable mode is found for $Re = 80$, with an eigenvalue $\lambda = \sigma - \imath\omega = 0.1018 - 0.7852\imath$. The streamwise velocity of the real part of this mode is shown in figure 3(*a*). The black line represents the stagnation-point streamline of the base flow, demarcating the recirculation region. The streamwise velocity $u^\dagger$ of the associated adjoint eigenmode is displayed in figure 3(*b*). As discussed in detail by Giannetti & Luchini (2007), Marquet *et al.* (2008) and others, the direct and adjoint eigenmode are localized upstream and downstream of the recirculation region, respectively.

2.2.2. *Nonlinear instability of the cylinder wake*

As the growing linear eigenmode reaches finite amplitude levels, the nonlinear terms become significant and the cylinder wake settles into a saturated periodically oscillating state, the Bénard–von Kármán vortex street. This time-periodic solution $\mathbf{q}_0(\mathbf{x}, t)$ is obtained numerically by time-marching the nonlinear equations with a semi-implicit second-order temporal discretisation, and a spatial discretisation identical to the one used for the eigenvalue problem. At each temporal iteration, an unsteady Stokes problem is

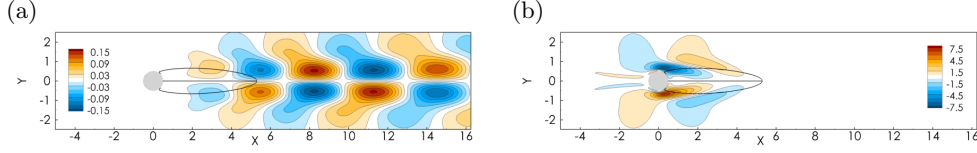(a)   (b)

FIGURE 3. Unstable linear eigenmode of the cylinder wake at $Re = 80$. The real frequency is $\omega_r = 0.785$, and the temporal growth rate is $\omega_i = 0.102$. a) streamwise velocity perturbations u of the direct eigenmode; b) adjoint streamwise velocity perturbations $u^\dagger$ of the associated adjoint mode. The black line indicates the recirculation region in the steady flow.

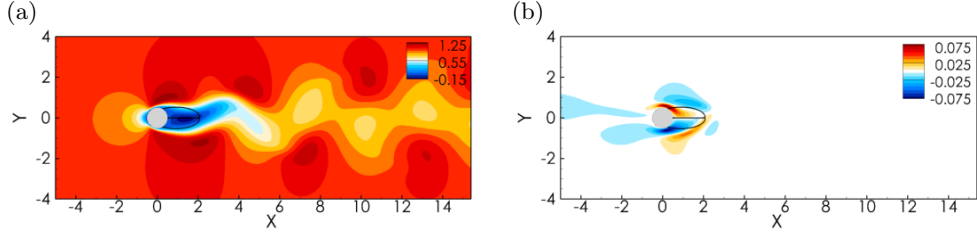(a)   (b)

FIGURE 4. Nonlinear global mode of the cylinder wake at $Re = 80$: a) total streamwise velocity $U + u$; b) adjoint streamwise velocity perturbations $u^\dagger$ of the associated adjoint Floquet mode. Both snapshots are taken at the same instant. The black line indicates the recirculation region in the mean flow.

solved with a preconditionned Uzawa algorithm (see Cuvelier *et al.* 1986) implemented in the FreeFem++ software. At $Re = 80$, the global frequency is found to be $\omega_g = 0.9957$, which is to be compared to the frequency of the linear eigenmode, $\omega = 0.7852$. The nonlinear correction to the global frequency is significant in this supercritical setting. A snapshot of the total streamwise velocity of the nonlinear global mode is shown in figure $4(a)$, where the black line now represents the stagnation-point streamline contour of the time-averaged flow. In the same way as discussed in §2.1.2 for the nonlinear Ginzburg–Landau equation, see (2.13, 2.23), an adjoint mode associated with the neutral Floquet mode of the nonlinear periodic state can be obtained by backward time-stepping of the adjoint tangential equation. Its streamwise velocity component $u^\dagger$ is shown in figure $4(b)$, taken at the same instant as the direct flow field in figure $4(a)$.

3. Active flow regions in linear global modes

3.1. *Sensitivity of the eigenvalue*

The sensitivity of an eigenvalue measures how this value varies in response to changes of the operator. In the present context, only *linear* sensitivities are considered, i.e. all variations are assumed to be infinitesimally small. If the original linear equation (2.2) has eigenmodes that satisfy $\lambda_j \mathcal{B} \phi_j = \mathcal{L} \phi_j$, a small perturbation $\epsilon \delta \mathcal{L}$ of the operator leads to a perturbed eigenvalue problem,

$$(\lambda_j + \epsilon \delta \lambda_j)\mathcal{B}(\phi_j + \epsilon \delta \phi_j) = (\mathcal{L} + \epsilon \delta \mathcal{L})(\phi_j + \epsilon \delta \phi_j),\qquad(3.1)$$

which at order ϵ can be rearranged to give

$$(\lambda_j \mathcal{B} - \mathcal{L})\,\delta \phi_j = -\delta \lambda_j \mathcal{B} \phi_j + \delta \mathcal{L}\,\phi_j\,.\qquad(3.2)$$

The Fredholm alternative states that this inhomogeneous problem in $\delta \phi_j$ has a solution if and only if the right-hand side term is orthogonal to the nullspace of the left-hand side operator, i.e. $\langle \phi_j^\dagger, -\delta \lambda_j \mathcal{B} \phi_j + \delta \mathcal{L}\,\phi_j \rangle = 0$. If the direct and adjoint modes are normalized

such that $\langle \boldsymbol{\phi}_j^\dagger , \mathcal{B} \boldsymbol{\phi}_j \rangle = 1$, this condition leads to

$$\delta \lambda_j = \langle \boldsymbol{\phi}_j^\dagger , \delta \mathcal{L} \, \boldsymbol{\phi}_j \rangle \,. \tag{3.3}$$

On the basis of (3.3), Giannetti & Luchini (2007) consider spatially localized perturbations of the operator,

$$\delta \mathcal{L} = \delta(\mathbf{x} - \mathbf{x}_0) \, \mathcal{C}_0 \,, \tag{3.4}$$

where $\mathcal{C}_0$ represents some artificially added coupling between the various flow variables at the location $\mathbf{x}_0$. If $\boldsymbol{\phi}_j(\mathbf{x}_0)$ and $\boldsymbol{\phi}_j^\dagger(\mathbf{x}_0)$ are understood to be vectors containing the n flow variable values at $\mathbf{x}_0$ ($n = 1$ for the Ginzburg–Landau equation and $n = 3$ for the cylinder wake), then $\mathcal{C}_0$ is represented by an $n \times n$ matrix, C_0, and the eigenvalue variation is obtained from (3.3) as

$$\delta \lambda_j \big|_{\mathbf{x}_0} = \boldsymbol{\phi}_j^{\dagger \star}(\mathbf{x}_0) \cdot \mathsf{C}_0 \cdot \boldsymbol{\phi}_j(\mathbf{x}_0) \,. \tag{3.5}$$

Taking the norm of C_0 to be unity without loss of generality, application of the Cauchy–Schwarz theorem yields an upper bound for the modulus of the eigenvalue variation, induced by an operator variation at $\mathbf{x}_0$ (Giannetti & Luchini 2007):

$$|\delta \lambda_j|_{\mathbf{x}_0} \leqslant \|\boldsymbol{\phi}_j^\dagger(\mathbf{x}_0)\| \, \|\boldsymbol{\phi}_j(\mathbf{x}_0)\| \,. \tag{3.6}$$

Marquet *et al.* (2008) define the operator variation in (3.3) specifically as being due to variations δU of the base flow, $\delta \mathcal{L} = (\nabla_U \mathcal{L}) \, \delta U$. This definition allows to quantify how a given small modification of the base flow, localized or distributed, alters the frequency ω and the growth rate σ. Both approaches represent the mathematical formulation of a well-posed question, based on different interpretations of what constitutes a 'wavemaker': in the case of Giannetti & Luchini (2007), it is the localized 'internal feedback' between perturbations, whereas in the case of Marquet *et al.* (2008) it is the feeding of perturbation growth on base flow energy. In both approaches, the answer is sought by probing the system with *exogenous* modifications of the operator structure.

3.2. *Endogeneity analysis of linear global modes*

With the question in mind how a localized region in the flow contributes to the global dynamics, we note that the admittance of any arbitrary operator $\mathcal{C}_0$ in (3.4) may be too general for the purpose of identifying the specific interactions that are inherent in the linear Navier–Stokes operator. Retaining the idea of considering the sensitivity of the eigenvalue with respect to *localized* changes of the operator, we stipulate that those changes preserve the local *structure* of the operator. This naturally leads to choosing

$$\delta \mathcal{L} = \delta(\mathbf{x} - \mathbf{x}_0) \, \mathcal{L} \,. \tag{3.7}$$

The variation of the operator at $\mathbf{x}_0$ is chosen to be proportional to the original operator itself in that same location. The sensitivity with respect to such variations quantifies directly how much the eigendynamics in a given point in space contribute to the frequency and to the growth rate; it is therefore suitable for an investigation of the *endogenous* global dynamics. We call this specific sensitivity

$$E(\mathbf{x}) = \boldsymbol{\phi}_j^{\dagger \star}(\mathbf{x}) \cdot \left(\mathcal{L} \boldsymbol{\phi}_j \right)(\mathbf{x}) \tag{3.8}$$

the *endogeneity* of the eigenmode $(\lambda_j, \boldsymbol{\phi}_j)$. Its computation is straightforward if the direct and adjoint eigenmodes as well as the operator are available. The dot-product in (3.8) again only denotes the scalar multiplication of two vectors containing the various state variables in one point in space.
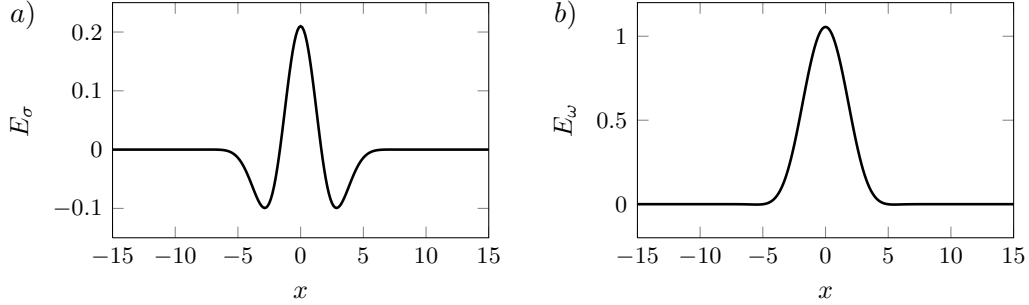
a)

b)

FIGURE 5. Endogeneity distribution of the leading linear Ginzburg–Landau eigenmode. (a) real part E_σ, related to growth rate, (b) negative imaginary part E_ω, related to frequency.

An essential property of the endogeneity is that its integral over $\mathbf{x}$ is equal to the eigenvalue λ_j:

$$\int_\Omega E(\mathbf{x})\mathrm{d}\mathbf{x} = \int_\Omega \phi_j^{\dagger\star} \cdot \left(\mathcal{L}\phi_j\right)\mathrm{d}\mathbf{x} = \langle\phi_j^\dagger, \mathcal{L}\phi_j\rangle = \langle\phi_j^\dagger, \lambda_j\mathcal{B}\phi_j\rangle = \lambda_j. \qquad (3.9)$$

It is important to note that, while any spatial distribution can be normalised to yield any integral scalar value, the endogeneity is the unique quantity that represents *local* contributions to the eigenvalue. For instance, the endogeneity allows to exclude any point in space from the integration, and the result reflects how the eigenvalue is altered due to the missing local contribution.

An endogeneity-based analysis clearly distinguishes between the promotion of unstable growth, contained in the real part of $E(\mathbf{x})$, and the frequency selection, given by the negative imaginary part. For the sake of clarity, let

$$E_\sigma(\mathbf{x}) = \Re\left[E(\mathbf{x})\right] \text{ and } E_\omega(\mathbf{x}) = -\Im\left[E(\mathbf{x})\right] \qquad (3.10)$$

be defined, such that $E(\mathbf{x}) = E_\sigma(\mathbf{x}) - \imath E_\omega(\mathbf{x})$, analogous to $\lambda = \sigma - \imath\omega$. The distinction between these two components is of great importance for a physical discussion, and the following examples will show that E_σ and E_ω in general present quite different spatial structures. Furthermore, with the definition (3.8) it is straightforward to decompose the operator $\mathcal{L}$, for instance into convection, diffusion and other terms, and to examine the individual contributions of these separate parts. Such a decomposition will be discussed in §3.4 for the cylinder wake.

3.3. *Example 1: linear Ginzburg–Landau equation*

The endogeneity formalism is first applied to the global instability modes shown in figure 1, with the parameters as given in § 2.1.1. Choosing $\mu_0 = \mu_c$, as defined by (2.22), the system is marginally unstable in a global sense. The endogeneity is found by multiplying $\phi^{\dagger*}$ with $\mathcal{L}\phi$ in every point x, where the eigenfunctions $\phi(x)$ and $\phi^\dagger(x)$ are given analytically by (2.20, 2.21), and the operator $\mathcal{L}$ is written out in (2.17).

Both parts of the endogeneity, E_σ and E_ω, are shown in figure 5: both are even functions, with their maximum values at $x = 0$. The integral of $E(x)$ is exactly equal to the associated eigenvalue, $\lambda = -4.398\imath$. In the $E_\sigma(x)$ distribution, shown in figure 5(a), negative and positive regions exactly counterbalance each other, totalling a zero growth rate. The largest contribution to both the frequency selection and the growth rate stems from the region around $x = 0$, not from regions where the magnitude of either the direct or adjoint eigenmodes is large (compare to figure 1).

This result is compared to the saddle point criterion given by Chomaz *et al.* (1991). In
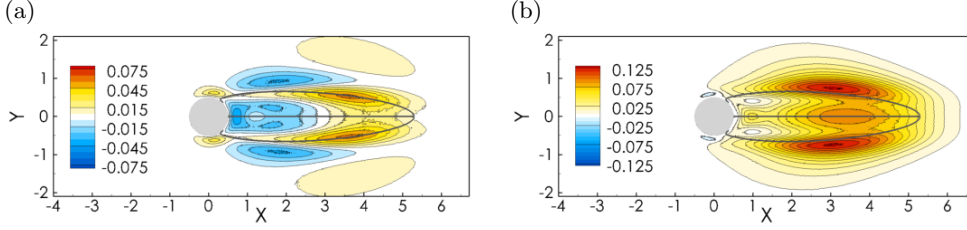
(a)

(b)

FIGURE 6. Endogeneity distribution of the linear cylinder wake instability. *a)* $E_\sigma(\mathbf{x})$, related to growth rate; *b)* $E_\omega(\mathbf{x})$, related to frequency. The spatial integral of E_σ equals the growth rate $\sigma = 0.102$, the spatial integral of E_ω equals the frequency $\omega = 0.785$.

their model, the 'wavemaker' location is defined by a saddle point of the local absolute frequency ω_0 in the complex x plane, $\partial_x \omega_0 = 0$. In the present case, one finds $\omega_0(x) = i\mu(x) - iU^2/4\gamma$, and therefore $\partial_x \omega_0 = i\partial_x \mu$, with a single saddle point precisely at $x = 0$. The 'wavemaker' location according to the criterion of Chomaz *et al.* (1991) is identical with the *maximally endogenous* location in this example. But whereas their WKBJ-based criterion identifies a singular location, the endogeneity quantifies contributions to the growth rate and the frequency from any point in the domain, thereby characterizing a distributed 'wavemaker'.

3.4. *Example 2: unstable linear global mode of the cylinder wake*

The endogeneity of the unstable linear eigenmode $\boldsymbol{\phi}$ of the cylinder wake, displayed in figure 3(a), is now examined. It is readily computed by point-wise multiplication of the complex conjugate of the adjoint eigenmode $\boldsymbol{\phi}^\dagger$, displayed in figure 3(b), with $\mathcal{L}\boldsymbol{\phi}$ where the definition of $\mathcal{L}$ is given in (2.25). As the divergence of perturbation velocity is zero in every point, the continuity equation along with the adjoint pressure $p^\dagger$ vanishes from the endogeneity definition, and one is left with

$$E(\mathbf{x}) = -\mathbf{u}^{\dagger *} \cdot [(\mathbf{u}_b \cdot \nabla)\mathbf{u}] - \mathbf{u}^{\dagger *} \cdot [(\mathbf{u} \cdot \nabla)\mathbf{u}_b] - \mathbf{u}^{\dagger *} \cdot \nabla p + Re^{-1} \mathbf{u}^{\dagger *} \cdot \Delta \mathbf{u}, \qquad (3.11)$$

where again it is understood that the left-hand side is to be evaluated in every point $\mathbf{x}$, such that all vectors only contain two scalar elements (x- and y-components). The endogeneity of the linear cylinder-wake instability mode is displayed in figure 6. The distribution of $E_\sigma(\mathbf{x})$, depicted in figure 6(a), shows where the temporal growth rate is generated, whereas $E_\omega(\mathbf{x})$, shown in figure 6(b), indicates how the various flow regions influence the global frequency selection.

A few general conclusions can be inferred from figure 6. Mainly, it is observed that the endogeneity (real and imaginary parts) is concentrated around the shear layers of the separation region, delimited in the figures by black lines. The frequency selection is clearly concentrated in two symmetric maximum locations. This part of the endogeneity resembles the quantity displayed by Giannetti & Luchini (2007) in their figure 17. The distribution of $E_\sigma(\mathbf{x})$ however bears a more faceted structure. Some regions are positive, contributing to global instability, others are negative, thus stabilising the eigenmode. The entire flow downstream of the separation region has practically no influence on frequency and growth rate, consistent with the conclusions of Giannetti & Luchini (2007) and Marquet *et al.* (2008).

A more insightful analysis of physical mechanisms may be based on a decomposition of the endogeneity into contributions from the various left-hand side terms in (3.11). In the given order, these terms account for the effects of base flow convection; production through base flow shear; pressure forces and diffusion. Their spatial distributions (real parts only, reflecting contributions to the growth rate) are shown in figure 7. The effect
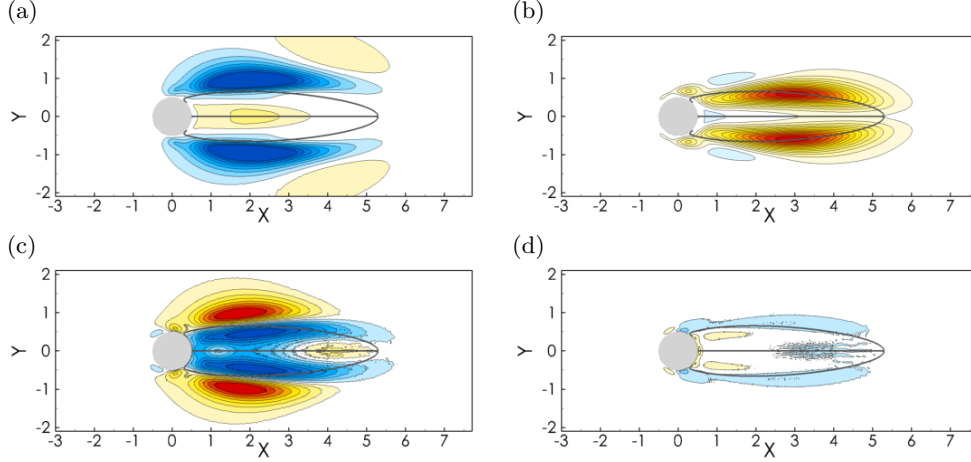
(a)

(b)

(c)

(d)

FIGURE 7. Real parts of the individual endogeneity terms in (3.11) (from left to right). *a)* Convection by the base flow; *b)* production through base flow shear; *c)* pressure forces; *d)* diffusion. The sum of these contributions gives $E_\sigma(\mathbf{x})$, shown in figure 6*a*. The same color scale is used here.

of convection by the base flow is dominantly stabilising (figure 7*a*). In the outer vicinity of the separation bubble, the downstream convection of perturbations counteracts their capacity of *in situ* growth, and renders the instability more convective. Inside the recirculation region, the upstream convection has the opposite effect. The production term (figure 7*b*) provides the principal source of global unstable growth.

The workings of pressure forces are not as obvious to interpret in physical terms, and their integrated net contribution to E_σ and E_ω is exactly zero in an incompressible setting. Since the adjoint velocity field is divergence-free, $\nabla \cdot \mathbf{u}^\dagger = 0$, it is easily found that

$$\int_\Omega \mathbf{u}^\dagger \cdot \nabla p \, \mathrm{d}\mathbf{x} = -\int_\Omega (\nabla \cdot \mathbf{u}^\dagger) \, p \, \mathrm{d}\mathbf{x} = 0 \tag{3.12}$$

Yet this term contributes strongly to the local values of the overall endogeneity. Tentatively, it may be argued that the role of the perturbation pressure gradient is to enforce the continuity condition, thereby causing a perturbation volume flux across the shear layer. As the instability perturbations tend to shorten the length of the separation bubble (manifest in the nonlinear mean flow), the stagnation-point streamline is forced toward the symmetry line, lessening the convective effect outside the bubble, and enhancing it inside.

The diffusion term is globally stabilizing, although inside the separation bubble near the cylinder it provokes a weak destabilisation. This seems to be the consequence of viscous transport of perturbation velocity into the shear layer. However low the amplitude of the diffusive contribution, it is crucial for accurately determining the instability threshold. The Reynolds number is expected to have two distinct effects on the instability. First, the stabilizing effect of the perturbation diffusion should weaken when the Reynolds number is increased. This is confirmed in figure 8(a), which shows the trends of the convection, production and diffusion contributions to the growth rate, as functions of the Reynolds number. The stabilizing diffusion effect lessens with increasing Reynolds number. Secondly, the steady base flow is influenced by the Reynolds number, affecting the instability mechanism via the production and convection terms. Individually, these contributions appear to be dominant, but with opposite effects on the growth rate. As
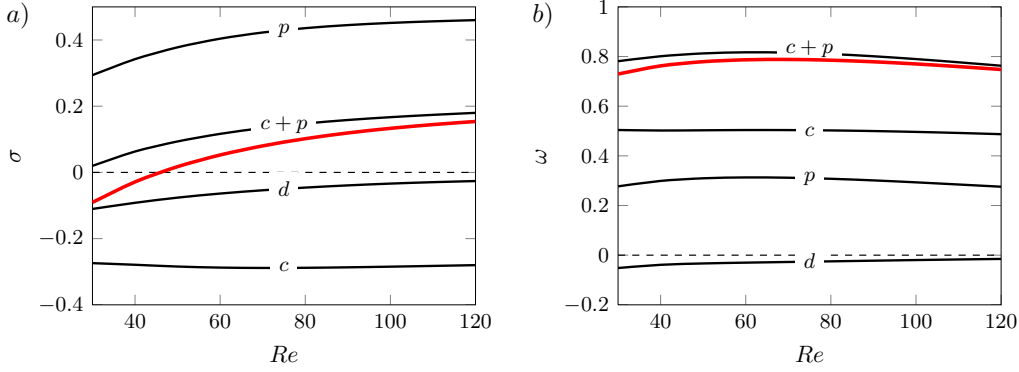
FIGURE 8. Net contributions of individual terms in the endogeneity definition (3.11), (*a*) to the linear growth rate, and (*b*) to the global frequency, as a function of the Reynolds number *Re*. Convection (-*c*-), production (-*p*-) and diffusion (-*d*-) contributions are shown, as well as the sum of convection and production ($c + p$) and the total values of σ and ω (thick red lines). The pressure gradient contribution is zero for all Reynolds numbers.

the Reynolds number is increased, the destabilisation by the production term overcomes the stabilisation by the convection term. The *combined* effect of these competing terms, represented by a line marked $c + p$ in figure 8(*a*), is then comparable in strength to the diffusion effect. On the other hand, the role of the diffusion in the frequency selection is all but negligible, as seen in figure 8(*b*). As for the growth rate, the dominant contributors are the production and convection terms. Both contribute here to increase the frequency. Their combined effect $(c + p)$ gives a good prediction of the linear frequency (red line), especially at high Reynolds number.

4. Active flow regions in nonlinear global modes

4.1. *Sensitivity of the global frequency*

The general sensitivity formulation for nonlinear time-periodic oscillations of a bifurcated flow state adopted here is similar to the analysis by Luchini *et al.* (2008), with some variations in the notation. Consider a nonlinear global mode $\mathbf{q}_0(\mathbf{x}, t)$, time-periodic solution of (2.1), with fundamental frequency ω_g. In order to make the frequency explicitly visible in the equation, the time variable is rescaled as $\tau = \omega_g t$, such that $\mathbf{q}_0(\mathbf{x}, \tau)$ is 2π-periodic in τ and satisfies

$$\omega_g \, \mathcal{B} \, \partial_\tau \mathbf{q}_0 = \mathcal{N}(\mathbf{q}_0) \, . \tag{4.1}$$

Just as in the linear case of §3.1, small variations of the left-hand side operator cause variations of the solution, including its frequency:

$$(\omega_g + \epsilon \delta \omega_g) \, \mathcal{B} \, \partial_\tau (\mathbf{q}_0 + \epsilon \delta \mathbf{q}_0) = (\mathcal{N} + \epsilon \delta \mathcal{N})(\mathbf{q}_0 + \epsilon \delta \mathbf{q}_0) \, . \tag{4.2}$$

With the introduction of the tangential linear operator $\mathcal{L}_{\mathbf{q}_0(t)}$ and its neutral Floquet mode $\boldsymbol{\psi}_1 = \partial_\tau \mathbf{q}_0$, defined in (2.10, 2.11), variations are governed at order ϵ by the relation

$$(\omega_g \mathcal{B} - \mathcal{L}_{\mathbf{q}_0(t)}) \, \delta \boldsymbol{\psi}_1 = -\delta \omega_g \, \mathcal{B} \, \boldsymbol{\psi}_1 + \delta \mathcal{N}(\mathbf{q}_0) \, , \tag{4.3}$$

The Fredholm alternative can be written out with the aid of the neutral adjoint Floquet mode $\boldsymbol{\psi}_1^\dagger$ (see §2), normalised to give $\{\boldsymbol{\psi}_1^\dagger, \mathcal{B} \boldsymbol{\psi}_1\} = 1$, which leads to

$$\delta \omega_g = \left\{ \boldsymbol{\psi}_1^\dagger, \delta \mathcal{N}(\mathbf{q}_0) \right\} \, . \tag{4.4}$$
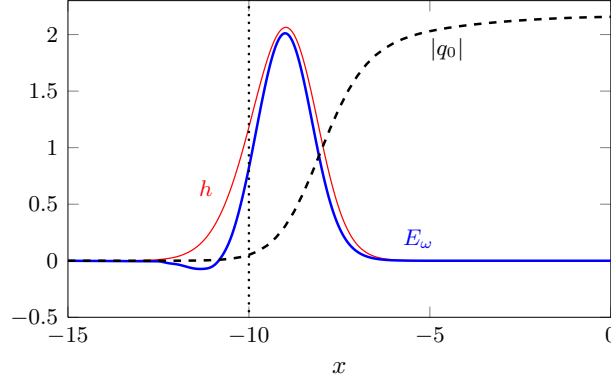
FIGURE 9. Endogeneity E_ω (thick blue line) of the nonlinear global mode of the Ginzburg—Landau equation, as shown in figure 2, compared with the quantity $h(x)$ (thin red line), which is obtained with the formalism described by Hwang (2015) according to (4.7). The dotted line marks the location x_{ca}, and the dashed line traces the envelope shape of the nonlinear global mode.

If $\boldsymbol{\psi}_1^\dagger$ is known, then the impact of any small operator variation $\delta\mathcal{N}$ on the global frequency can be immediately evaluated from (4.4). In practice, $\boldsymbol{\psi}_1^\dagger$ is obtained in the following way: first, the nonlinear equation is numerically integrated by time-stepping until the periodic nonlinear global mode regime is fully attained. Then the (linear) adjoint tangential equation is stepped backwards in time, starting from an arbitrary initialization, over as many cycles of the nonlinear global mode as necessary. During this backward-in-time integration, the adjoint solution converges asymptotically towards the sought-after neutral mode.

4.2. *Endogeneity analysis of nonlinear global modes*

Analogously to the linear case in § 3.2, the endogeneity of a nonlinear global mode is defined by considering variations of the nonlinear operator that preserve its structure but are localized in space, and also in time, since the nonlinear operator is time-dependent,

$$\delta\mathcal{N} = \delta(\mathbf{x} - \mathbf{x}_0)\delta(\tau - \tau_0)\mathcal{N}. \tag{4.5}$$

The inner product in (4.4) involves integration in $\mathbf{x}$ as well as in τ. Integration over the Dirac functions yields the expression for the influence of spatio-temporal variations in the operator on the frequency selection,

$$E_\omega(\mathbf{x}, \tau) = \Re\left[\boldsymbol{\psi}_1^{\dagger*}(\mathbf{x}, \tau) \cdot \mathcal{N}(\mathbf{q}_0(\mathbf{x}, \tau))\right]. \tag{4.6}$$

Only the frequency selection in nonlinear global modes is considered at present, because it is assumed here that both quantities, in practice, are obtained from a flow solver in the form of real-valued variables. The scaled time τ denotes the temporal phase within an oscillation cycle.

4.3. *Example 1: the nonlinear Ginzburg–Landau equation*

The nonlinear global mode and its neutral adjoint Floquet mode of the Ginzburg–Landau equation (figure 2) have been discussed in §2.1.2. The associated endogeneity, according to (4.6), is shown in figure 9. It is noted that the endogeneity is independent of τ in the present case of the Ginzburg–Landau equation.

The E_ω distribution is nonzero in a narrow region around $x = -9$, and its integral in

x and over one period $0 \leqslant \tau \leqslant 2\pi$ is exactly equal to the global frequency, $\omega_g = 3.70$. According to Pier *et al.* (1998), the global frequency of a nonlinear Ginzburg–Landau system with slowly varying coefficients is selected at the location x_{ca}, where the local instability changes from upstream convective to downstream absolute. In the limit of marginal global instability, the global frequency is then predicted to correspond to the absolute frequency at x_{ca}. In the present example, one finds $x_{ca} = -10$, and the absolute frequency at this location is $\omega_0(x_{ca}) = 4.50$. The chosen parameter configuration (see §2.1) is strongly globally unstable, and the parameter μ varies significantly in x around x_{ca}, therefore the present case does not respect the limiting assumptions of Pier *et al.* (1998), and the frequency prediction is quite inaccurate as a result. The endogeneity however provides a clear and accurate picture of the frequency selection process. The maximum contribution to the global frequency is found at $x = -9$, indeed not far from the 'wavemaker' location x_{ca} as defined by Pier *et al.* (1998).

The present results may be compared to the structural sensitivity of nonlinear global modes as defined by Hwang (2015), who adapted the formulation of Luchini *et al.* (2008) to analyze nonlinear global modes of the Ginzburg–Landau equation. According to Hwang (2015), worst-case variations of the global frequency due to added 'closed-loop perturbations' (synonymous to 'internal feedback'), written in the notation of this paper, are characterized by the spatial distribution

$$h(x) = \left| \frac{q_0^*(x)\, \psi_1^\dagger(x)}{N} \right|, \quad \text{with} \quad N = \int_0^T \int_{-\infty}^{\infty} (\psi_1^{\dagger *}\, q_0 - \psi_1^\dagger\, q_0^*)\, \mathrm{d}x\, \mathrm{d}t\,. \tag{4.7}$$

Figure 9 compares this distribution, multiplied with $2\omega_g$ for consistent scaling, with the endogeneity E_ω. The two curves are very similar, and in particular the position of their maxima is identical. Again it is pointed out that the analysis of Hwang (2015), in contrast to the endogeneity formalism, considers modifications of the operator that do not preserve its original structure.

In conclusion, just as in the linear analysis of §3.2, the results obtained from the nonlinear endogeneity analysis are consistent with the 'wavemaker' definition from classical asymptotic theory, but they go further in a quantitative description of the dynamics, because the endogeneity fully accounts for the effects of non-parallelism and supercriticality. It is also consistent with recent formulations that describe the structural sensitivity, but it reveals the endogenous dynamics that are specific to the operator under consideration.

4.4. *Example 2: Nonlinear frequency selection in the cylinder wake*

The endogeneity of the time-periodic flows developing in the wake of the circular cylinder, described in §2.2.2, is explicitly obtained as

$$E_\omega(\mathbf{x}, \tau) = \mathbf{u}_1^\dagger \cdot \left[-(\mathbf{u}_0 \cdot \nabla)\mathbf{u}_0 - \nabla p_0 + Re^{-1}\Delta \mathbf{u}_0 \right], \tag{4.8}$$

where $\mathbf{q}_0(\mathbf{x}, \tau) = (\mathbf{u}_0, p_0)$ is the 2π-periodic nonlinear solution and $\mathbf{u}_1^\dagger$ is the velocity component of the 2π-periodic solution of the linear adjoint equation.

The spatio-temporal endogeneity (4.8) is integrated over one oscillation cycle, and the result, shown in figure 10, demonstrates that the endogenous region resembles a front, localized around $x = 2$. Similarly to the earlier observations in the context of the Ginzburg-Landau equation, the endogenous region of the nonlinear global mode in the cylinder wake is located further upstream than that of its linear counterpart (compare to figure 6b). The separation line of the recirculation regions both in the base flow and in the time-averaged mean flow are depicted by grey and black lines, respectively, in figure 10. Interestingly, the endogenous region of the nonlinear global mode appears to
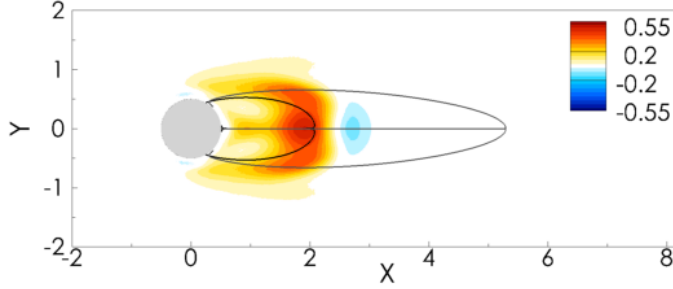
FIGURE 10. Time-integrated endogeneity $E_\omega(\mathbf{x})$ of the nonlinear global mode in the cylinder wake at $Re = 80$. The nonlinear frequency is $\omega_g = 0.995$. The black (resp. grey) lines indicate the recirculation region in the time-averaged mean flow (resp. base flow).

be supported by the recirculation region in the mean flow, as opposed to the base flow. This observation suggests that further investigation of the nonlinear dynamics should focus on the analysis of fluctuations around the mean flow state.

To this aim, the nonlinear global mode state is first decomposed as $\mathbf{q}_0 = \bar{\boldsymbol{q}} + \mathbf{q}'$ into a time-averaged component $\bar{\boldsymbol{q}} = (\bar{\boldsymbol{u}}, \bar{p})^T$ and a zero-mean fluctuation component $\mathbf{q}' = (\mathbf{u}', p')^T$. Introducing this decomposition into the Navier-Stokes operator (2.24), and time-averaging over one oscillation cycle, one obtains the steady nonlinear equations that govern the mean flow,

$$(\bar{\boldsymbol{u}} \cdot \nabla)\bar{\boldsymbol{u}} + \nabla\bar{p} - Re^{-1}\Delta\bar{\boldsymbol{u}} = -\overline{(\boldsymbol{u}' \cdot \nabla)\boldsymbol{u}'}, \tag{4.9}$$

$$\nabla \cdot \bar{\boldsymbol{u}} = 0. \tag{4.10}$$

By subtraction, the unsteady nonlinear equations for the fluctuations are obtained as

$$\omega_g\, \partial_\tau \boldsymbol{u}' + (\bar{\boldsymbol{u}} \cdot \nabla)\boldsymbol{u}' + (\boldsymbol{u}' \cdot \nabla)\bar{\boldsymbol{u}} + \nabla p' - Re^{-1}\Delta\boldsymbol{u}' = -(\boldsymbol{u}' \cdot \boldsymbol{\nabla})\boldsymbol{u}' + \overline{(\boldsymbol{u}' \cdot \boldsymbol{\nabla})\boldsymbol{u}'}, \tag{4.11}$$

$$\nabla \cdot \boldsymbol{u}' = 0. \tag{4.12}$$

The right-hand side forcing terms both in (4.9) and in (4.11) arise from the nonlinear interaction of fluctuations. The temporal mean of $(\boldsymbol{u}' \cdot \boldsymbol{\nabla})\boldsymbol{u}'$ forces the mean flow, whereas its zero-mean fluctuation forces the flow fluctuations. At small amplitudes of $\boldsymbol{u}'$, these terms are negligible, such that the steady and unsteady equations reduce to the base flow and linear perturbation equations. By contrast, when a linear eigenmode experiences exponential growth and reaches finite amplitude levels, the effect of the forcing terms in (4.9) and (4.11) will become significant. The right-hand side in (4.9) drives the base flow towards the mean flow. The right-hand side in (4.11) modifies the dynamics of the fundamental oscillations at frequency ω_g, and it generates harmonic components at integer multiples of ω_g. Thus the effect of nonlinearity on the frequency selection can be attributed to two distinct origins. The first is a nonlinear deformation of the mean flow, which in turn modifies the left-hand side linear operator in (4.11). The second one is the nonlinear interaction of fluctuation harmonics, induced by the right-hand side forcing term in (4.11).

The endogeneity definition (4.8) is now expanded in terms of mean flow and fluctuation
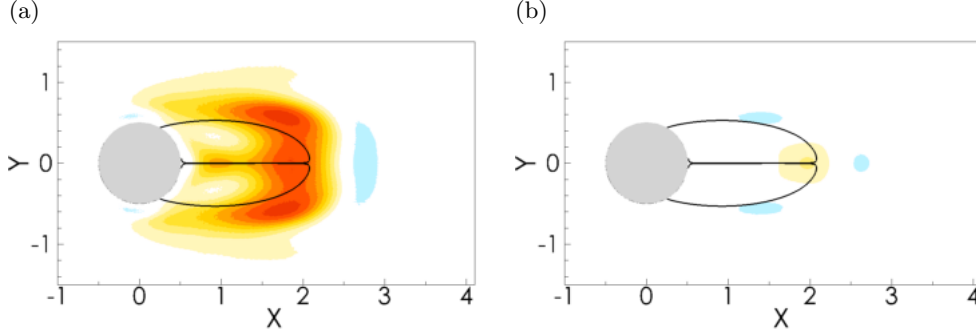
(a) (b)

FIGURE 11. Contributions to the time-integrated endogeneity of the nonlinear global mode. (a) Quasi-linear dynamics around the mean flow defined by (4.15) and (b) interaction between high harmonical components defined by (4.15). The color bar shown in figure 10 is also used here. The black line indicates the recirculating flow region in the mean flow. $Re = 80$.

components. With this decomposition, as developed above, one obtains

$$E_\omega(\mathbf{x}, \tau) = \mathbf{u}^\dagger \cdot \left[-(\bar{\boldsymbol{u}} \cdot \nabla)\bar{\boldsymbol{u}} - \nabla\bar{p} + Re^{-1}\Delta\bar{\boldsymbol{u}} - \overline{(\mathbf{u}' \cdot \nabla)\mathbf{u}'} \right] \tag{4.13}$$

$$+ \mathbf{u}^\dagger \cdot \left[-(\bar{\mathbf{u}} \cdot \nabla)\mathbf{u}' - (\mathbf{u}' \cdot \nabla)\bar{\mathbf{u}} - \nabla p' + Re^{-1}\Delta\mathbf{u}' \right]$$

$$+ \mathbf{u}^\dagger \cdot \left[-(\mathbf{u}' \cdot \nabla)\mathbf{u}' + \overline{(\mathbf{u}' \cdot \nabla)\mathbf{u}'} \right].$$

The first line in the above equation vanishes because the expression in square brackets is the momentum equation for the mean flow (4.9. By further splitting the adjoint velocity into mean and fluctuation components, denoted $\bar{\boldsymbol{u}}^\dagger$ and $\boldsymbol{u}^{\dagger'}$ respectively, the time-integrated endogeneity simplifies to

$$\int_0^{2\pi} E_\omega(\mathbf{x}, \tau)\, d\tau = \int_0^{2\pi} E_m(\mathbf{x}, \tau)\, d\tau + \int_0^{2\pi} E_h(\mathbf{x}, \tau)\, d\tau, \tag{4.14}$$

with

$$E_m(\mathbf{x}, \tau) = \boldsymbol{u}^{\dagger'} \cdot \left(-(\bar{\mathbf{u}} \cdot \nabla)\mathbf{u}' - (\mathbf{u}' \cdot \nabla)\bar{\mathbf{u}} - \nabla p' + Re^{-1}\Delta\mathbf{u}' \right), \tag{4.15}$$

$$E_h(\mathbf{x}, \tau) = \boldsymbol{u}^{\dagger'} \cdot \left(-(\mathbf{u}' \cdot \nabla)\mathbf{u}' + \overline{(\mathbf{u}' \cdot \nabla)\mathbf{u}'} \right), \tag{4.16}$$

All contributions involving the mean adjoint velocity vanish. The component $E_m(\boldsymbol{x}, \tau)$ highlights spatial regions where the quasi-linear dynamics around the mean flow contribute to the frequency selection, whereas $E_h(\boldsymbol{x}, \tau)$ identifies regions where the interaction of harmonic components influences the global frequency.

The time-integrated components E_m and E_h, for the nonlinear global mode in the cylinder wake at $Re = 80$, are shown in figure 11. The sum of these two contributions, according to (4.14), gives the time-integrated frequency endogeneity displayed in figure 11. In the present configuration, the frequency selection process is clearly dominated by the quasi-linear dynamics around the mean flow, whereas harmonic interactions contributes only very weakly. The total contributions

$$\omega_m = \int_\Omega \int_0^{2\pi} E_m(\mathbf{x}, \tau)\, d\tau\, d\boldsymbol{x}, \quad \omega_h = \int_\Omega \int_0^{2\pi} E_h(\mathbf{x}, \tau)\, d\tau\, d\boldsymbol{x}, \tag{4.17}$$

are reported in table 1 for various values of the Reynolds number. For all values of the Reynolds number investigated in this study, the contribution ω_m of the quasi-linear mean flow dynamics to the global frequency is greater than 97%.

Re	ω	ω_g	$\omega_m(\%)$	$\omega_h(\%)$
50	0.7676	0.8159	0.8087 (99.1)	0.0072 (0.9)
75	0.7742	0.9726	0.9543 (98.1)	0.0182 (1.9)
80	0.7852	0.9957	0.9768 (98.1)	0.0189 (1.9)
100	0.7553	1.0703	1.0493 (98.0)	0.0210 (2.0)
125	0.7246	1.1382	1.1127 (97.7)	0.0255 (2.3)
150	0.6896	1.1922	1.1596 (97.2)	0.0325 (2.8)

TABLE 1. Endogeneity-based decomposition of the nonlinear global mode frequency, for various values of the Reynolds number Re. Linear eigenmode frequency ω of the base flow; nonlinear global mode frequency ω_g; contributions to ω_g from quasi-linear dynamics in the mean flow (ω_m) and from harmonic interaction (ω_h), as defined by (4.17).

This result explains a posteriori why a global stability analysis of the time-averaged flow accurately predicts the frequency of the time-periodic vortex shedding in the cylinder wake (Barkley 2006). Mantic-Lugo *et al.* (2014) recently proposed a self-consistent nonlinear model based on the marginal stability of the mean flow, which accurately determines both the mean flow and the frequency of the vortex shedding in the cylinder wake. However, the influence of higher harmonics in the frequency selection of nonlinear instability is not negligible in all circumstances. Indeed, Turton *et al.* (2015) recently showed that in thermosolutal convection driven by opposite thermal and solutal gradients, oscillation frequencies of *travelling* convection waves can be predicted from stability analysis of the mean flow, but not those of *standing* waves. The application of endogeneity analysis to the thermosolutal convection problem is not attempted here, but it is expected to reveal a stronger influence of the harmonic interactions in the frequency selection of standing waves.

Finally, a decomposition of the endogeneity component (4.15) similar to the demonstration in §3.4 characterizes the contributions of the various terms to the quasi-linear dynamics. For $Re = 80$, the contributions of production and mean flow convection to the global frequency are displayed in figures 12*a,b*, and the contributions of diffusion and pressure gradient are shown in figures 12*c,d*. The production contribution is dominant, concentrated in the shear layers of the mean recirculation region. Inside this region, the action of the pressure gradient further increases the frequency. Table 2 summarizes all total contributions, ω_m^p, ω_m^c, ω_m^d, of the production, convection and diffusion terms at various Reynolds numbers . The net integral of the pressure gradient term is always identically zero. At all Reynolds numbers, the effects of diffusion and mean flow convection approximately compensate each other, and their balance is small compared to the strong contribution of the production term.

5. Conclusions

A novel sensitivity formalism has been introduced, named the endogeneity, which allows to precisely quantify the influence of each point in the flow field on the global frequency selection and on the promotion of unstable growth, both in the context of linear temporal eigenmodes and of nonlinear global modes. Its application has been demonstrated for the Ginzburg–Landau equation and for the wake of a circular cylinder, in linear as well as nonlinear settings. The results obtained have been shown to be consistent with earlier 'wavemaker' definitions, in particular the WKBJ-based saddle point criterion of Chomaz *et al.* (1991) and the structural sensitivities defined by Giannetti &

(a)   (b)

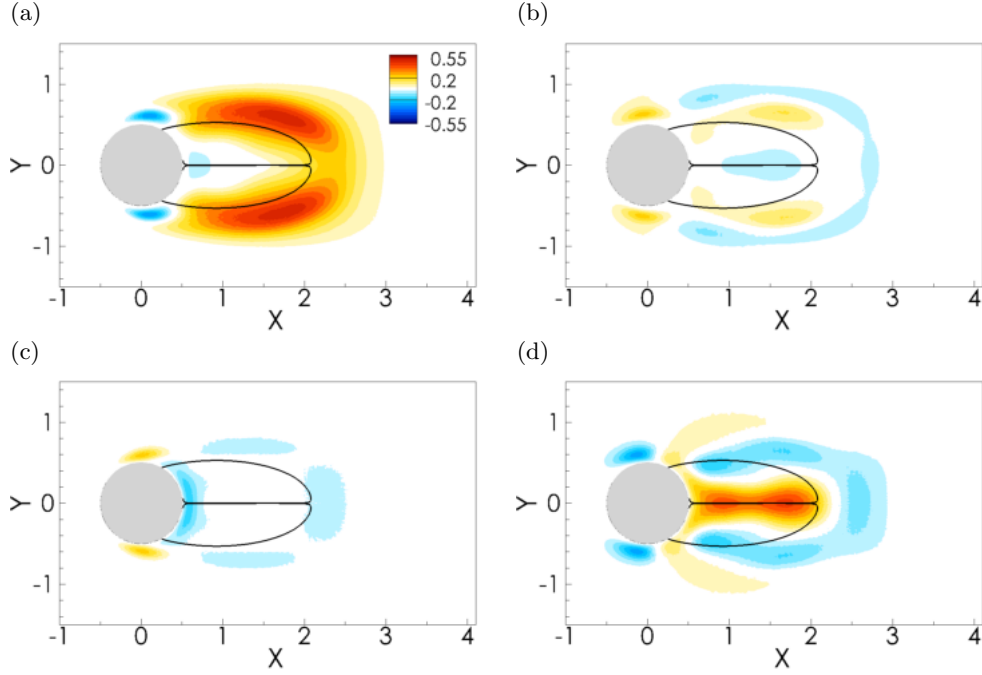(c)   (d)

FIGURE 12. Spatial distribution of various contributions to the endogeneity of the quasi-linear mean flow dynamics: (a) production by the mean flow, (b) convection by the mean flow, (c) diffusion and (d) pressure gradient. The black line delimits the recirculation region in the mean flow.

Re	ω_m	ω_m^p	ω_m^c	ω_m^d
50	0.8087	0.9997	0.0023	−0.1933
75	0.9543	0.9435	0.1567	−0.1459
80	**0.9768**	**0.9482**	**0.1679**	**-0.1394**
100	1.0493	0.9999	0.1696	−0.1203
125	1.1127	1.0989	0.1224	−0.1087
150	1.1596	1.1721	0.0853	−0.0978
175	1.1935	1.2220	0.0604	−0.0889

TABLE 2. Decomposition of the quasi-linear contribution to the fresquency into three contributions: the production term ω_m^p, convection term ω_m^c and diffusion term ω^d in the quasi-linear mean flow dynamics.

Luchini (2007), Luchini *et al.* (2008) and Hwang (2015). The novel aspect with respect to the latter sensitivity approaches arises from the specific form of operator variations that are considered: the endogeneity characterizes the sensitivity of the eigenvalue with respect to localized operator variations that preserve the specific structure of the original operator. This sensitivity may therefore be interpreted as the *local contribution* of any point in the flow field to the global eigendynamics, in terms of frequency selection and unstable growth. Contributions to these two parts of the eigenvalue are clearly distinguished, contained separately in the real and imaginary parts of the endogeneity. Further analysis of the role of individual terms of the operator follows naturally within this framework. In particular, a decomposition of a nonlinear flow operator into time-averaged and

fluctuating parts gives insight into the role of quasi-linear dynamics developing on the mean flow versus the nonlinear interaction of harmonic fluctuation components. This latter part of the analysis, exemplified for the case of the cylinder wake, has important implications for the characterisation of nonlinear time-periodic flow states, in relation to recent investigations (Mantic-Lugo *et al.* 2014; Turton *et al.* 2015).

Appendix A. Influence of the inner product

The question may arise whether and how the choice of an inner product different from (2.9) affects the endogeneity definition. In particular, many flow problems are investigated in cylindrical coordinates, where the standard inner product includes the radial coordinate r as part of the volume element. For practical purposes, the procedure is outlined here for *discrete* eigenvalue problems, with a generalized inner product.

Let $\tilde{\phi}_j$ be a discrete representation of the linear eigenfunction ϕ_j, in a discrete space where the inner product $\langle \phi_1, \phi_2 \rangle$ between two flow states is expressed as $\tilde{\phi}_1^H Q \tilde{\phi}_2$. The matrix Q is typically diagonal, with real elements that represent volume elements of the mesh, and possibly any further weight functions. It will only be assumed here that Q is invertible, but even this condition can be relaxed with some additional effort.

The discrete direct and adjoint eigenvalue problems are defined by

$$-\iota\omega_j B \tilde{\phi}_j = L \tilde{\phi}_j \,, \tag{A 1}$$

$$\iota\omega_j^* Q^{-1,H} B^H Q^H \tilde{\phi}_j^\dagger = Q^{-1,H} L^H Q^H \tilde{\phi}_j^\dagger \,. \tag{A 2}$$

The matrix $Q^{-1,H}$ on both sides of (A 2) can be omitted. It is found that $\check{\phi}_j^\dagger = Q^H \tilde{\phi}_j^\dagger$ is the adjoint eigenvector satisfying

$$\iota\omega_j^* B^H \check{\phi}_j^\dagger = L^H \check{\phi}_j^\dagger \,. \tag{A 3}$$

Let $\mathbf{\Phi}_j(\mathbf{x}_k)$ be defined as the vector $\mathbf{\Phi}_j(\mathbf{x}_k) = \delta(\mathbf{x} - \mathbf{x}_k) L \tilde{\phi}_j$ for convenient writing, where $\mathbf{x}_k$ denotes the discrete mesh points. The endogeneity definition, written in terms of discrete vectors and operators, is then

$$-\iota E(\mathbf{x}_k) = \langle \phi_j^\dagger, \delta(\mathbf{x} - \mathbf{x}_k) \mathcal{L} \phi_j \rangle = \tilde{\phi}_j^{\dagger H} Q \mathbf{\Phi}_j(\mathbf{x}_k) = \check{\phi}_j^{\dagger H} \mathbf{\Phi}_j(\mathbf{x}_k). \tag{A 4}$$

It follows from (A 4) that the endogeneity is invariant with respect to the choice of the inner product. This holds true also for the example of cylindrical coordinates: it seems unnecessary to account for the r factor. Without the need to specify a Q matrix, $E(\mathbf{x}_k)$ may be computed directly from the discrete adjoint eigenvector, obtained from the transpose conjugate problem (A 3). This will generally be the simplest option.

REFERENCES

BARKLEY, D. 2006 Linear analysis of the cylinder wake mean flow. *Europhys. Lett.* **75**, 750–756.

CHOMAZ, J.-M. 2003 Fully nonlinear dynamics of parallel wakes. *J. Fluid Mech.* **495**, 57–75.

CHOMAZ, J.-M., HUERRE, P. & REDEKOPP, L.G. 1987 Models of hydrodynamic resonances in separated shear flows. In *Proceedings of the Sixth Symposium on Turbulent Shear Flows, Toulouse, France*, pp. 321–326.

CHOMAZ, J.-M., HUERRE, P. & REDEKOPP, L.G. 1988 Bifurcations to local and global modes in spatially developing flows. *Phys. Rev. Lett.* **60**, 25–28.

Chomaz, J.-M., Huerre, P. & Redekopp, L.G. 1991 A frequency selection criterion in spatially developing flows. *Stud. Appl. Math* **84** (2), 119–144.

Cossu, C. & Chomaz, J.-M. 1997 Global measures of local convective instabilities. *Phys. Rev. Lett.* **78** (23), 4387.

Couairon, A. & Chomaz, J.-M. 1997 Absolute and convective instabilities, front velocities and global modes in nonlinear systems. *Physica D* **108**, 236–276.

Cuvelier, C., Segal, A. & Van Steenhoven, A. 1986 *Finite element methods and Navier-Stokes equations*, , vol. 22. Reidel, Dordrecht, Netherlands.

Giannetti, F. & Luchini, P. 2007 Structural sensitivity of the first instability of the cylinder wake. *J. Fluid Mech.* **581**, 167–197.

Huerre, P. 2000 Open shear flow instabilities. In *Perspectives in Fluid Dynamics* (ed. G. K. Batchelor, H. K. Moffatt & M. G. Worster), pp. 159–229. Cambridge University Press.

Huerre, P. & Monkewitz, P.A. 1990 Local and global instabilities in spatially developing flows. *Annu. Rev. Fluid Mech.* **22**, 473–537.

Hwang, Y. 2015 Structural sensitivities of soft and steep nonlinear global modes in spatially developing media. *Eur. J. Mech. B/Fluids* **49B**, special issue: "Trends in Hydrodynamic Instabilities".

Iooss, G. & Joseph, D. 1997 *Elementary stability and bifurcation theory*. Springer, New York.

Koch, W. 1985 Local instability characteristics and frequency determination of self-excited wake flows. *J. Sound Vib.* **99** (1), 53–83.

Luchini, P. & Bottaro, A. 2014 Adjoint equations in stability analysis. *Annu. Rev. Fluid Mech.* **46**, 493–517.

Luchini, P., Giannetti, F. & Pralits, J. 2008 Structural sensitivity of linear and nonlinear global modes. *AIAA Paper* **2008-4227**.

Mantic-Lugo, V., Arratia, C. & Gallaire, F. 2014 Self-consistent mean flow description of the nonlinear saturation of the vortex shedding in the cylinder wake. *Phys. Rev. Lett.* **113**, 407–417.

Marquet, O., Sipp, D. & Jacquin, L. 2008 Sensitivity analysis and passive control of cylinder flow. *J. Fluid Mech.* **615**, 221–252.

Monkewitz, P. 1990 The role of absolute and convective instability in predicting the behavior of fluid systems. *Eur. J. Mech. B/Fluids* **9**, 395–413.

Pier, B. 2002 On the frequency selection of finite-amplitude vortex shedding in the cylinder wake. *J. Fluid Mech.* **458**, 407–417.

Pier, B. & Huerre, P. 2001 Nonlinear self-sustained structures and fronts in spatially developing wake flows. *J. Fluid Mech.* **435**, 145–174.

Pier, B., Huerre, P., Chomaz, J.-M. & Couairon, A. 1998 Steep nonlinear global modes in spatially developing media. *Phys. Fluids* **10**, 2433–2435.

Provansal, M., Mathis, C. & Boyer, L. 1987 Bénard–von Kármán instability: transient and forced regimes. *J. Fluid Mech.* **182**, 1–22.

van Saarlos, W. 1988 Front propagation into unstable states: marginal stability as dynamical mechanism for velocity selection. *Phys. Rev. A* **37**, 211–229.

van Saarlos, W. 1989 Front propagation into unstable states: II. linear versus nonlinear marginal stability and rate of convergence. *Phys. Rev. A* **39**, 6367–6390.

Sipp, D. & Lebedev, A. 2007 Global stability of base- and mean-flows: a general approach and its applications to cylinder and open cavity flows. *J. Fluid Mech.* **593**, 333–358.

Turton, S. E., Tuckerman, L. S. & Barkley, D. 2015 Prediction of frequencies in thermosolutal convection from mean flows. *Phys. Rev. E* **91**, 043009.